

A new scheme for designing the penalty factor in 3-D penalty-equilibrating mixed elements

Yan Ping Cao^{1,3}, Ning Hu^{2,*},†, Jian Lu¹, Hisao Fukunaga² and Zhen Han Yao³

¹*LASMIS, Université de technologie Troyes 12, rue Marie Curie-BP 2060-10010 Troyes cedex, France*

²*Department of Aeronautics and Space Engineering, Tohoku University, 01 Aramaki-Aoba, Aoba-ku, Sendai 980-8579, Japan*

³*Department of Engineering Mechanics, Tsinghua University, Beijing 100084, People's Republic of China*

SUMMARY

In this paper, a new scheme for designing the penalty factor in 3-D penalty-equilibrating mixed elements based on the Hu–Washizu three-field variational functional is proposed to improve the performance of the elements when applied to beam, plate and shell structures. In order to construct this new scheme, the role played by the penalty factor is first discussed in detail by comparing it with the selective reduced factor designed by Sze for overcoming the so-called ‘trapezoid locking’. The reason of the poor performance of the penalty-equilibrating element for the distorted elemental geometry is investigated thoroughly. Furthermore, the penalty factor is designed to alleviate the influence of false strain/stress in elements by considering the geometrical characteristics of beam, plate and shell structures. The new scheme is applied to the penalty-equilibrating 3-D mixed element proposed by the present authors previously. Some challenging numerical examples are selected to demonstrate the effectiveness of the present approach. Copyright © 2004 John Wiley & Sons, Ltd.

KEY WORDS: three-field variational principle; penalty factor; 3-D mixed element; mesh distortion

1. INTRODUCTION

The application of low-order 3-D solid elements without rotational degree of freedoms to thin plate/shell analyses has aroused considerable interests. The reasons are that they are simpler in their geometric and kinetic descriptions, the laborious task of introducing algebraic constraints or solid-to-shell transition elements can be excluded, and the complication on handling finite rotations can be avoided. In some recent studies, for instance, Weissman [1] has applied a high accurate brick element to the plate and shell problems. For regular meshes, this brick element can provide good results to the shell or plate elements, but for irregular meshes the accuracy decreases greatly. Sze *et al.* [2] proposed a selective-reduced strategy to improve the

*Correspondence to: Ning Hu, Department of Aeronautics and Space Engineering, Tohoku University, 01 Aramaki-Aoba, Aoba-ku, Sendai 980-8579, Japan.

†E-mail: hu@ssl.mech.tohoku.ac.jp

performance of the hybrid stress element for beam, plate and shell problems. Sze *et al.* [3] also proposed a hybrid stress ANS solid-shell element and generalized it successfully to the smart structure modelling. This element cannot pass the patch test for the solid element, but it is still acceptable since it was mainly designed for the plate/shell structures. Recently, Sze *et al.* [4] have presented a modified generalized laminate stiffness matrix method to resolve the thickness locking and some abnormalities encountered by solid-shell elements in laminate analysis. Based on the work of Wu and Cheung [5] for the hybrid stress element, we have proposed a penalty-equilibrating 3-D mixed element for the elastic [6] and elasto-plastic [7] analyses from the Hu–Washizu three-field variational principle. In this paper, for beam, plate and shell problems, a new scheme for designing the penalty factor in our previous penalty-equilibrating 3-D mixed element [6, 7] has been proposed to improve the performance of elements possessing distorted geometrical shapes. This technique can also be applied to the penalty-equilibrating hybrid stress element [5].

2. COMPARISON BETWEEN THE PENALTY FACTOR AND SELECTIVE-REDUCED FACTOR

In this section, we compare the similar roles played by the penalty factor in the penalty-equilibrating elements and by the selective-reduced factor proposed in Reference [8], which can provide useful information for the design of the penalty factor.

First, we start from the penalty-equilibrating hybrid stress element [5], which was based on the following two-field variational principle,

$$\pi_{\text{H-R}}^e = \int_{\Omega} \left(-\frac{1}{2} \boldsymbol{\sigma}^T \mathbf{C}^{-1} \boldsymbol{\sigma} + \boldsymbol{\sigma}^T \boldsymbol{\varepsilon} - \alpha (\nabla \cdot \boldsymbol{\sigma})^T (\nabla \cdot \boldsymbol{\sigma}) \right) dV - \pi_{\text{EXT}}^e \quad (1)$$

where α is the penalty factor. It should be pointed out that α is not a non-dimensional variable, this problem has been discussed and solved in References [7, 8] for 2-D and 3-D cases, respectively. Consider the dimension of α , we write it in the following form:

$$\alpha = \gamma l_0^2 \quad (2)$$

where γ is a large positive non-dimensional number. About the definition of l_0 , one can refer to Reference [8] for 2-D problems and Reference [7] for 3-D problems.

By taking the interpolation functions of stress $\boldsymbol{\sigma}$ and strain $\boldsymbol{\varepsilon}$ as those in Reference [2], the stiffness matrix can be expressed as

$$\mathbf{k}^e = 4j_0 \mathbf{B}_c^T \mathbf{C} \mathbf{B}_c + \begin{bmatrix} \mathbf{G}_1 \\ \mathbf{G}_2 \end{bmatrix}^T \left(\begin{bmatrix} H_{11} & \mathbf{0} \\ \mathbf{0} & H_{22} \end{bmatrix} + \frac{\gamma l_0^2}{E} \begin{bmatrix} H_{11}^p & H_{12}^p \\ H_{21}^p & H_{22}^p \end{bmatrix} \right)^{-1} \begin{bmatrix} \mathbf{G}_1 \\ \mathbf{G}_2 \end{bmatrix} \quad (3)$$

To investigate the ‘trapezoidal locking’ problem, one typical element as shown in Figure 1, has been selected, which has also been used by Sze [8] to present his scaling technique for a five-beta hybrid-stress element.

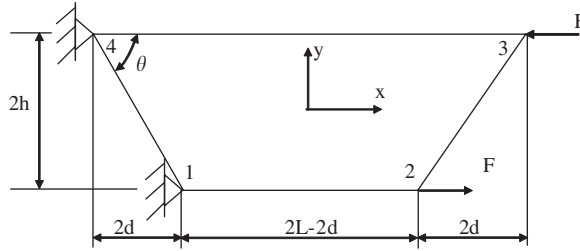


Figure 1. A typical trapezoid element.

Taking ξ to be aligned with the neutral axis, the stiffness can be rewritten as

$$\mathbf{k}^e = 4\mathbf{j}_0 \mathbf{B}_c^T \mathbf{C} \mathbf{B}_c + \begin{bmatrix} \mathbf{G}_1 \\ \frac{1}{\sqrt{\gamma}} \mathbf{G}_2 \end{bmatrix}^T \left(\begin{bmatrix} H_{11} & 0 \\ 0 & \frac{1}{\gamma} H_{22} \end{bmatrix} + \frac{l_0^2}{E} \begin{bmatrix} 0 & 0 \\ 0 & H_{22}^p \end{bmatrix} \right)^{-1} \begin{bmatrix} \mathbf{G}_1 \\ \frac{1}{\sqrt{\gamma}} \mathbf{G}_2 \end{bmatrix} \quad (4)$$

According to the explanation of Sze [8], to overcome the locking caused by the parasitic strain in the problem shown in Figure 1, \mathbf{G}_2 matrix should be scaled by one parameter like $1/\sqrt{\gamma}$ shown here. Also, if η is aligned with the neutral axis, there is the following relationship:

$$\begin{bmatrix} H_{11}^p & H_{12}^p \\ H_{21}^p & H_{22}^p \end{bmatrix} = \begin{bmatrix} H_{11}^p & 0 \\ 0 & 0 \end{bmatrix} \quad (5)$$

and the stiffness matrix is

$$\mathbf{k}^e = 4\mathbf{j}_0 \mathbf{B}_c^T \mathbf{C} \mathbf{B}_c + \begin{bmatrix} \frac{1}{\sqrt{\gamma}} \mathbf{G}_1 \\ \mathbf{G}_2 \end{bmatrix}^T \left(\begin{bmatrix} \frac{1}{\gamma} H_{11} & 0 \\ 0 & H_{22} \end{bmatrix} + \frac{l_0^2}{E} \begin{bmatrix} H_{11}^p & 0 \\ 0 & 0 \end{bmatrix} \right)^{-1} \begin{bmatrix} \frac{1}{\sqrt{\gamma}} \mathbf{G}_1 \\ \mathbf{G}_2 \end{bmatrix} \quad (6)$$

Then, \mathbf{G}_1 matrix has been scaled to eliminate the parasitic strain and overcome the ‘trapezoidal locking’.

Sze [8] has presented a selective-reduced scheme to make the PS element [9] be free of ‘trapezoidal locking’. The stiffness matrix of the modified PS element is

$$\mathbf{k}_{\text{sze}}^e = 4\mathbf{j}_0 \mathbf{B}_c^T \mathbf{C} \mathbf{B}_c + \begin{bmatrix} \chi_1 \mathbf{G}_1 \\ \chi_2 \mathbf{G}_2 \end{bmatrix}^T \left(\begin{bmatrix} H_{11} & 0 \\ 0 & H_{22} \end{bmatrix} \right)^{-1} \begin{bmatrix} \chi_1 \mathbf{G}_1 \\ \chi_2 \mathbf{G}_2 \end{bmatrix} \quad (7)$$

where

$$\frac{1}{\chi_1} = \sqrt{1 + \kappa \left(\frac{a_3^2 + b_3^2}{a_1^2 + b_1^2} \frac{j_1}{j_0} \right)^2}, \quad \frac{1}{\chi_2} = \sqrt{1 + \kappa \left(\frac{a_1^2 + b_1^2}{a_3^2 + b_3^2} \frac{j_2}{j_0} \right)^2} \quad (8)$$

and κ is a large non-dimensional value.

Without loss of the generality, taking ξ to be aligned with the neutral axis, we can get $\chi_1 = 1$ and

$$\frac{1}{\chi_2} = \sqrt{1 + \kappa \frac{L^2 d^2}{h^4}} \quad (9)$$

Equation (7) becomes

$$\mathbf{k}_{\text{size}}^e = 4\mathbf{j}_0 \mathbf{B}_c^T \mathbf{C} \mathbf{B}_c + \begin{bmatrix} \mathbf{G}_1 \\ \chi_2 \mathbf{G}_2 \end{bmatrix}^T \left(\begin{bmatrix} H_{11} & 0 \\ 0 & H_{22} \end{bmatrix} \right)^{-1} \begin{bmatrix} \mathbf{G}_1 \\ \chi_2 \mathbf{G}_2 \end{bmatrix} \quad (10)$$

Comparing Equation (4) with Equation (10), we can see the similar roles played by the penalty factor and the selective-reduced factor. A further analysis will be made in the following to find the difference between these two factors. Taking the penalty factor in the penalty-equilibrating element [5] as $\alpha = 10^4$, here $\alpha = 10^4$ is a value with dimension, from Equation (2), we have

$$\gamma = \frac{10^4}{l_0^2} \quad (11)$$

Furthermore, by taking ξ to be aligned with the neutral axis in Figure 1, and $l_0^2 = j_0 = Lh$ as advised in Reference [8], the following relationship can be obtained:

$$\gamma = \frac{10^4}{Lh} \quad (12)$$

By means of Equations (9) and (12), we have

$$\frac{\sqrt{\gamma}}{\left(\frac{1}{\chi_2}\right)} = \frac{10^2}{\sqrt{Lh + \kappa(d^2 L^3/h^3)}} \quad (13)$$

From Figure 1 it can be seen that $d = h/\tan(\theta)$. Taking $\kappa = 10^4$ and fixing $h = 1$, the right-hand term in Equation (13) is plotted in Figure 2 by changing L . From this figure, we can find that with the increase of L/h , the values of two factors differ from each other gradually, e.g. when $L/h > 5$, $\sqrt{\gamma} < 1/\chi_2$ in Figure 2, when $L/h > 10$, in Figure 2, $\sqrt{\gamma} \ll 1/\chi_2$.

According to Figure 2, we can draw a conclusion that the accuracy of the penalty-equilibrating element [5] is significantly affected by the change of elemental geometry, e.g. the increase of L/h . This phenomenon can be seen in Table 2 of Reference [8].

Bearing this in mind, we will present a new scheme for designing the penalty factor in the penalty-equilibrating elements for the analysis of beam, plate and shell.

3. A NEW SCHEME FOR DESIGNING THE PENALTY FACTOR

As the analysis in the previous section, the penalty factor in the previous penalty-equilibrating elements [5, 6] did not involve the effect of the geometry of element. Hence based on the above discussion, in this section, we proposed a new scheme for the selection of penalty factor in 3-D penalty elements for the analysis of beam, plate and shell.

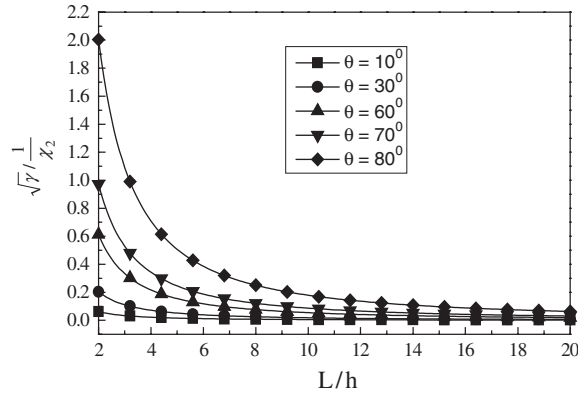


Figure 2. $\sqrt{\gamma}/(1/\chi_2)$ vs L/h for various θ .

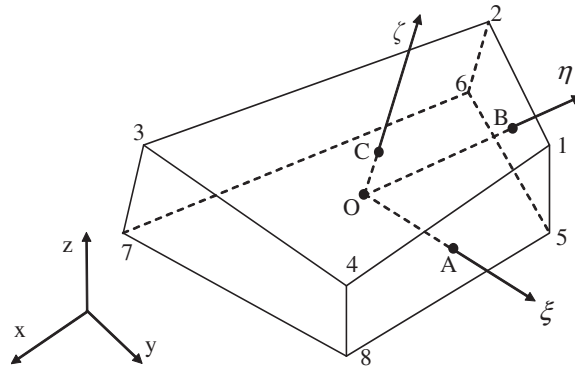


Figure 3. A typical solid element.

First, for a typical brick element shown in Figure 3, we assume that the penalty factor can be expressed as

$$p_x = g(E, \kappa, l_1, l_2, l_3) \tag{14}$$

where E is the Young's modulus, κ is a large positive number (10^3 – 10^5 is advised) and l_1, l_2 and l_3 are defined as

$$\begin{aligned} l_1 &= |OA| = \sqrt{a_1^2 + b_1^2 + c_1^2} \\ l_2 &= |OB| = \sqrt{a_2^2 + b_2^2 + c_2^2} \\ l_3 &= |OC| = \sqrt{a_3^2 + b_3^2 + c_3^2} \end{aligned} \tag{15}$$

where

$$\begin{bmatrix} a_1 & b_1 & c_1 \\ a_2 & b_2 & c_2 \\ a_3 & b_3 & c_3 \end{bmatrix} = \frac{1}{8} \begin{bmatrix} 1 & -1 & -1 & 1 & 1 & -1 & -1 & 1 \\ 1 & 1 & -1 & -1 & 1 & 1 & -1 & -1 \\ 1 & 1 & 1 & 1 & -1 & -1 & -1 & -1 \end{bmatrix} \begin{Bmatrix} x_1 & y_1 & z_1 \\ \vdots & \vdots & \vdots \\ x_8 & y_8 & z_8 \end{Bmatrix} \quad (16)$$

Secondly, the penalty factor is taken as

$$p_\alpha = \frac{\kappa}{E} l_0^2 f(l_1, l_2, l_3) \quad (17)$$

where l_0 is introduced to eliminate the dimension in the penalty factor [5], its definition is given in Reference [7] as $l_0 = \frac{1}{3}(l_1 + l_2 + l_3)$.

Based on the discussion in the previous section and Reference [2], for plate and shell problems, e.g. $l_1 \approx l_2 \gg l_3$, we define function f as follows:

$$f(l_1, l_2, l_3) = \frac{l_1 l_2}{l_3^2} \quad (18)$$

The corresponding penalty factor is

$$p_{\alpha_{\text{shell}}} = \frac{\kappa l_0^2 l_1 l_2}{E l_3^2} \quad (19)$$

For beam problems, e.g. $l_1 \gg l_2 \approx l_3$, function f is given as

$$f(l_1, l_2, l_3) = \frac{l_1^2}{l_2 l_3} \quad (20)$$

The corresponding penalty factor is

$$p_{\alpha_{\text{beam}}} = \frac{\kappa l_1^2 l_0^2}{E l_2 l_3} \quad (21)$$

This penalty factor can be used in our previous penalty-equilibrating mixed element [6]. It can also be easily applied to the penalty-equilibrating hybrid stress element [5]. About the judgment of the geometry of element, a simple scheme has been proposed in Reference [2], it is also adopted in the present work.

4. NUMERICAL EXAMPLES

In this section, some numerical examples have been chosen to test the performance of the proposed scheme for the design of the penalty factor in the penalty-equilibrating element. All the elements referred to in this paper for comparison are listed as follows:

- PT: 3-D hybrid stress element proposed by Pian and Tong [10].
- SS18 β : 3-D hybrid stress element proposed by Sze *et al.* [2].
- WE: 3-D mixed element proposed by Weissman [1].
- PWE: 3-D penalty-equilibrating mixed element proposed by the present authors [6].

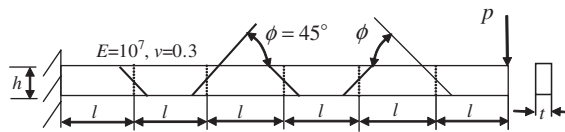
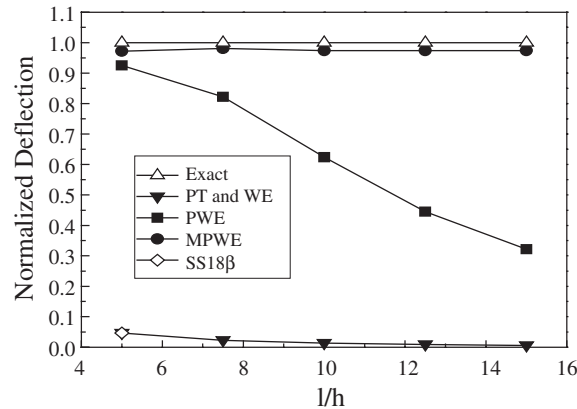


Figure 4. MacNeal–Harder beam.


 Figure 5. Normalized deflection at the tip vs l/h .

MPWE: 3-D penalty-equilibrating mixed element by means of the new scheme for designing the penalty factor, the parameter κ in Equations (19) and (21) is taken as $\kappa = 10^4$.

4.1. MacNeal and Harder beam [11]

A beam modeled by six elements is subjected to a unit shear load (Figure 4). The geometric parameters of the beam, h , t and ϕ are fixed, but the length of the element (l) is changed. The results of the normalized deflection at the tip obtained from four different elements are plotted against the changing of the parameter l/h as shown in Figure 5. The results are normalized with the analytical solution: $0.1081l^3$. From Figure 5, it can be seen that the MPWE element presents very good results in this test. It should be pointed out that the result of SS18 β element is directly taken from Reference [2]. Trapezoidal locking is caused by the normal transverse strain modes, which have been scaled in Reference [2]. If the scaling factor is properly taken in the construction of elemental stiffness, trapezoidal locking can also be resolved.

4.2. Clamped thin circular plate

This example is a clamped thin circular plate of radius $R = 5$, subjected to a unit concentrated load at the center. The thickness of the plate changes from 0.01 to 0.2. Due to the symmetry of the plate, only one quarter of the plate is analysed with 48 elements as shown in Figure 6. The material parameters are $E = 10920.0$, $\nu = 0.3$. This problem is usually modelled using some typical plate elements, here it is taken to show the performance of the proposed 3-D element in plate problems. The normalized deflection at the centre changing with the thickness

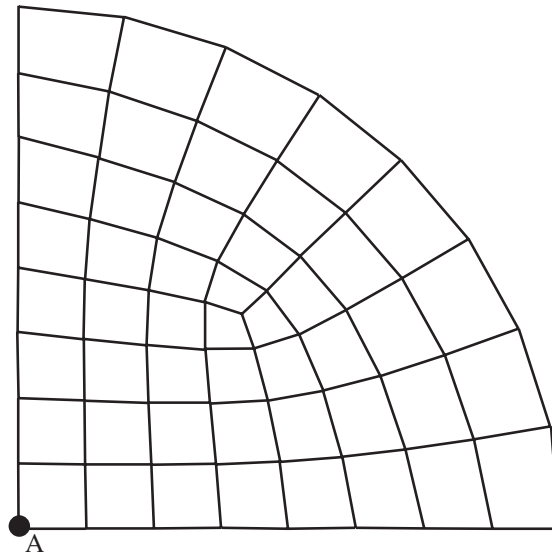
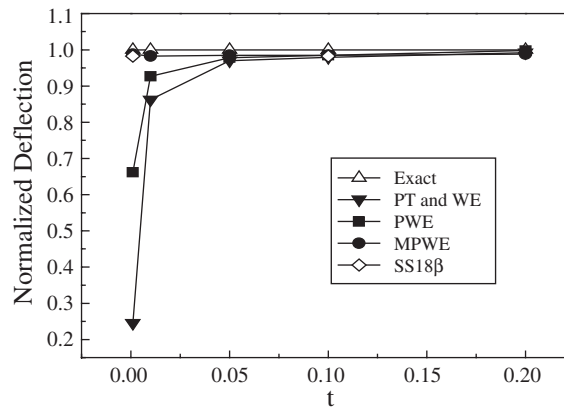


Figure 6. A clamped thin circular plate.

Figure 7. Normalized deflection at the center of the plate vs plate thickness t .

of the plate is shown in Figure 7. The MPWE and SS18 β elements perform the best. They are not sensitive to the change of the thickness of the plate.

4.3. A pipe penetrating a big plate

A structure shown in Figure 8 is analysed using the present MPWE element and the PT element. The material constants used in the analysis are $E = 21000.0$, $\nu = 0.3$. The inner radius of the pipe is 2 and its thickness is 3. A coarse FEM mesh for the present and PT elements

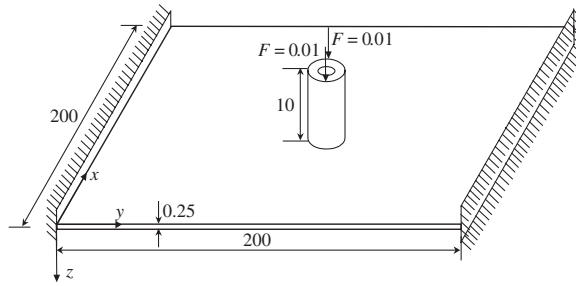


Figure 8. A pipe penetrating a big plate.

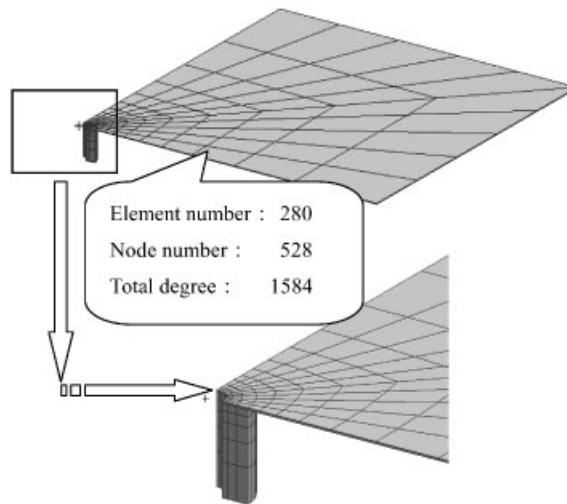


Figure 9. Coarse finite element mesh for MPWE and PT elements.

Table I. Comparison between the maximum displacements under the load points on the pipe in the z -axis direction obtained from MPWE and PT elements and that of HEXA8 element by using a refined mesh.

	MPWE (coarse mesh)	PT (coarse mesh)	HEXA8 (refined mesh)
Maximum displacement in the z -axis direction	0.181	0.137	0.190
	0.181	0.137	0.190

is given in Figure 9. This example demonstrates the flexibility of the MPWE element for modelling the 3-D solid and plate structures simultaneously. Table I lists the maximum displacement in the z -axis direction under the load points obtained from MPWE element and PT element. The results obtained from the HEXA8 element in NASTRAN [12] by using refined meshes of 22858 elements and 43104 nodes is also provided for comparison. The present

element exhibits the obviously superior performance compared with the PT element. Therefore, through this example, it is obvious that the MPWE element can be selected as a powerful alternative of the plate or shell elements. For the structures with the geometrical characteristics of both solid and plate or shell portions, the traditional analysis usually employs the solid and shell elements simultaneously and introduces the displacement constraints or solid-to-shell transition elements to guarantee the displacement conforming between two portions. When using the present element directly for both solid and plate or shell portions, this laborious task in the traditional approach can be excluded.

5. CONCLUSIONS

In this paper, in order to improve the performance of the penalty-equilibrating mixed or hybrid elements when applied to beam, plate and shell problems, a new scheme for designing the penalty factor has been proposed. The main idea of the scheme is to introduce a geometric parameter, which is related to the shape of the element, into the penalty factor. Then, with the change of the elemental geometry, the penalty factor can be automatically adjusted and the false strains in the element can be controlled effectively. This new scheme is used to improve the performance of the penalty-equilibrating mixed element proposed previously by the present authors, the numerical examples have justified its effectiveness.

REFERENCES

1. Weissman SL. High-accuracy low-order three-dimensional brick elements. *International Journal for Numerical Methods in Engineering* 1996; **39**:2337–2361.
2. Sze KY, Ghali A. Hybrid hexahedral element for solids, plates, shells and beams by selective scaling. *International Journal for Numerical Methods in Engineering* 1993; **22**:1519–1540.
3. Sze KY, Yao LQ. A hybrid-stress ANS solid-shell element and its generalization to smart structure modelling—part I: solid-shell element formulation, part II: smart structure modeling. *International Journal for Numerical Methods in Engineering* 2000; **48**:545–582.
4. Sze KY, Lo SH, Yao LQ. Hybrid-stress solid elements for shell structures based upon a modified variational functional. *International Journal for Numerical Methods in Engineering* 2002; **53**:2617–2642.
5. Wu C-C, Cheung YK. On optimization approaches of hybrid elements. *Finite Elements in Analysis and Design* 1995; **21**:111–128.
6. Cao YP, Hu N, Lu J, Fukunaga H, Yao ZH. A 3-D brick element based on Hu-Washizu variational principle for mesh distortion. *International Journal for Numerical Methods in Engineering* 2002; **53**:2529–2548.
7. Cao YP, Hu N, Fukunaga H, Lu J, Yao ZH. A highly accurate brick element based on a three-field variational principle for elasto-plastic analysis. *Finite Elements in Analysis and Design* 2003; **39**:1155–1171.
8. Sze KY. On immunizing five-beta hybrid-stress element models from ‘trapezoidal locking’ in practical analyses. *International Journal for Numerical Methods in Engineering* 2000; **47**:907–920.
9. Pian THH, Sumihara K. Rational approach for assumed stress finite elements. *International Journal for Numerical Methods in Engineering* 1984; **20**:1685–1695.
10. Pian THH, Tong P. Relations between incompatible displacement model and hybrid stress model. *International Journal for Numerical Methods in Engineering* 1986; **22**:173–181.
11. MacNeal RH, Harder RL. A proposed standard set of problems to test finite element accuracy. *Finite Elements in Analysis and Design* 1985; **1**:3–20.
12. NASTRAN. Theory Manual, MSC Inc, 2001.